PROCEEDINGS OF SCIENCE

ONLINE ICRC 2021
THE ASTROPARTICLE PHYSICS CONFERENCE
Berlin | Germany
37th International Cosmic Ray Conference
12–23 July 2021

The Energy Scale Calibration Using the Moon Shadow of LHAASO-WCDA Detector

Yanjin Wang,[a,*] **Zhen Cao,**[b] **Zongkang Zeng,**[b] **Lingling Ma**[b] **and Yuncheng Nan**[c] **on behalf of the LHAASO Collaboration**
(a complete list of authors can be found at the end of the proceedings)

[a] *College of Sciences, Northeastern University,*
110819 Shenyang, Liaoning, China
[b] *Key Laboratory of Particle Astrophysics & Experimental Physics Division, Institute of High Energy Physics, Chinese Academy of Sciences,*
100049 Beijing, China
[c] *Institute of Frontier and Interdisciplinary Science, Shandong University,*
266237 Qingdao, Shandong, China
E-mail: wangyanjin@ihep.ac.cn, caozh@ihep.ac.cn, zengzk@ihep.ac.cn, llma@ihep.ac.cn, nanyc@ihep.ac.cn

The Water Cherenkov Detector Array (WCDA) of LHAASO are designed to work in combination for measuring the energy spectra of the cosmic ray species over a very wide energy range from a few TeV to 10 PeV. The energy calibration can be achieved with a proven technique of measuring the westward shift of Moon shadow cast by galactic cosmic rays due to the geomagnetic field. This deflection angle Δ is inversely proportional to the cosmic ray rigidity. The precise measurement of the shifts by WCDA allows us to calibrate its energy scale for energies as high as 35 TeV. In this work, we demonstrate the feasibility of the method using the data collected from May 2019 to January 2020 by WCDA-1, the first of the three water Cherenkov ponds, already commissioned at the LHAASO site.

**** 37th International Cosmic Ray Conference (ICRC2021), ****
**** 12-23 July 2021 ****
**** Berlin, Germany - Online ****

[*] Presenter

© Copyright owned by the author(s) under the terms of the Creative Commons Attribution-NonCommercial-NoDerivatives 4.0 International License (CC BY-NC-ND 4.0).

PoS(ICRC2021)356

1. Introduction

The energy spectrum measurement is very important to reveal the origin and acceleration mechanism of cosmic ray. In recent years, there are some ground base experiments for the cosmic ray measurement such as a scintillation counter array, water Cherenkov detectors, or imaging air Cherenkov telescopes However, there are some difficulties in energy spectrum measurement for cosmic rays with energies higher than 10TeV. Therefore, results of different energy spectrum measurement experiments are not very consistent, which may be caused by uncertainty of the absolute energy scale. So, it is mandatory to establish a way to calibrate the shower energy measurement between the different detectors, a non-trivial task given that it has to be done directly using cosmic ray data. Many experiments, such as ARGO-YBJ [1], have successfully calibrated their energy-scale by using the deficit of cosmic rays blocked by Moon, which is called Moon shadow. The geo-magnetic-field (GMF), deflecting the charged cosmic rays, shifts Moon shadow on the ground with respect to Moon real position. The displacement of the shadow is clearly dependent on the rigidity. and becomes negligible at high energies. However, at energies below 40 TeV the shadow shift westward is clearly observable.

The Water Cherenkov Detector Array (WCDA) of the Large High Altitude Air Shower Observatory (LHAASO) has a detection threshold of about 1 TeV for cosmic rays. WCDA has measured Moon shadow shifts as a function of $N_{\rm pe}$. Here $N_{\rm pe}$ is the total number of photo-electrons measured by units with trigger time within 30 ns from the shower conical front. A data set has been collected from 01/05/2019 to 31/01/2020 with 731.2 hours of Moon observation with zenith angle smaller than 45°. The reconstruction of arrival directions and shower cores is described in reference [2]. To obtain the significance of the shadowing effect, events with cores located both inside and outside the pond 1 are used. The significance of Moon shadow for each $N_{\rm pe}$ group is greater than 10σ.

In this work, firstly we briefly describe the LHAASO observatory detectors in section 2. In section 3, we introduced the measurement of Moon shadow shifts for high energy showers. It is shown the calculation of Moon shadow shifts by raytracing in GMF from simulation in section 4 In 4, we discuss how the energy scale for WCDA-1 can be established using Moon shadow shift measurement for energies above 6 TeV. The uncertainties of the energy scale are also discussed in the section.

2. The LHAASO WCDA arrays

The LHAASO Observatory is based on the so-called 'hybrid' approach for the measurement of shower characteristics, consisting in the simultaneous detection of atmospheric showers with different types of detectors. The observatory is built around the three ponds of water Cherenkov Detector Array (WCDA), featuring 3120 gap-less detecting units to instrument an area of 78,000 m^2. Near WCDA 18 wide field of view Cherenkov telescopes (WFCTA) are installed. They survey the sky above the whole array with a coverage of 4608 square degrees [3] [4] . This core of the array is surrounded by 5195 scintillation counters (ED) and 1188 muon detectors (MD), which constitute an array covering an area of 1 km^2 (KM2A) [3] [4]. The construction of LHAASO has nearly been completed.

PoS(ICRC2021)356

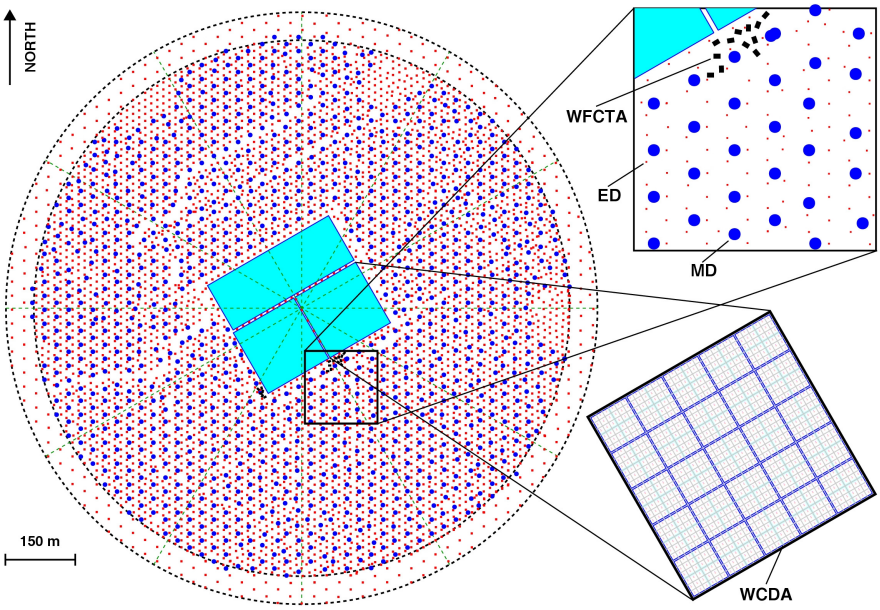

Figure 1: The LHAASO layout. The three ponds of WCDA are represented by the cyan rectangles at the center of the site, each divided into 900 square cells of 5×5 m^2 grouped into 25 clusters (as can be seen in the zoomed view at the bottom right). The 18 WFCTA telescopes, positioned near the WCDA, can be seen in the zoomed view at the top right. The remaining KM2A extends over an area of about 1 km^2, instrumented with the electromagnetic detector (ED) array of scintillation counters (small red dots) and the muon detector array (big blue dots).

As shown in Fig. 1, WCDA is composed of two ponds with an area of 150 m $\times$ 150 m each and a third larger one with an area of 300 m $\times$ 110 m. The smaller pond in the South-West direction, named WCDA-1, has started science operations since April 2019. It has 900 units, or cells, of 25 m^2, each equipped with a large (8") PMT used also for timing and a small (1.5") PMT at the center of each unit at 4.4 m of depth from the water surface. The use of two PMTs watching upwards allows us to cover a wide dynamic range spanning from 1 to 200,000 photo-electrons, which are generated by the Cherenkov light produced in water by the shower charged secondary particles. To suppress the light cross-talking effect and improve the timing resolution, black plastic curtains delimit the units. The front-end electronics (FEE) of the large PMTs is designed to achieve a time resolution of 0.5 ns eought to reconstruct the shower front conical structure. The large dynamic range provided by the combined operation of PMTs enables the measurement of the particle density distribution in the shower cores without any saturation even for energetic showers up to 10 PeV. This allows to measure the core location with a precision better than 3 m over a wide energy range. WCDA-1 can measure shower directions with a resolution better than 0.2° above 10 TeV and 1.0° above 600 GeV [2]. The water transmission can be monitored by the 'muon' peak observed by each unit [2].

PoS(ICRC2021)356

3. Measurement of Moon shadow shifts

The selection of energy parameter for Moon shadow and energy scale analysis is very important. $N_{\rm pe}$ may represent a robust estimator up to very high energies [2] which is a good proxy for energy in this work. The distribution of $N_{\rm pe}$ is shown in Fig. 2 when $N_{\rm hit}$ greater than 100, 200, or 300. We can learn that the efficiency of the range measured is high when $N_{\rm pe}$>50,000. Showers reconstructed in WCDA-1 with $N_{\rm hit}$ more than 200 have a good angular resolution of 0.39° [2].

Datas used for Moon shadow analysis are selected from 01/05/2019 to 31/01/2020. The total effective observation time of Moon is 731.2 hours and the total number of events is about 4.17 million with arrival direction within 5° to the normal Moon position. The standard reconstruction procedure has been adopted, all reconstruction data with $N_{\rm hit}$ more than 200 and the zenith angles smaller than 45°. Samples are grouped into 6 groups according to $N_{\rm pe}$ as shown in Table 1. In the analysis, the equal zenith angle method [5] is used and the sky map is divide into a grid of $0.02^\circ \times 0.02^\circ$. The significance calculation in each grid is estimated by Li & Ma formula [6] in this work. For the $N_{\rm pe}$ group with $N_{\rm pe} > 60,000$, a significance as high as 10.9 σ can be achieved

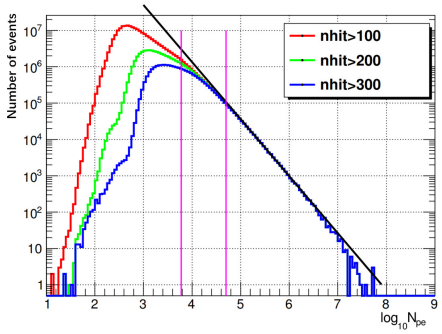

Figure 2: The distribution of the total number of photo-electrons, $N_{\rm pe}$, for shower events coming from a region around the normal Moon position. The histograms in red, green and blue correspond to events with number of hit cells, $N_{\rm hit}$, greater than 100, 200 and 300, respectively. The black solid line indicates a power law $\propto N_{\rm pe}^{-2.6}$, which fits the histograms for $N_{\rm pe} > 50,000$. The two vertical magenta lines indicate the range used for the energy calibration using Moon shadow.

as shown in Fig. 3. The deficit number of events map can be obtained by the difference between source on and source off window, After casting shadow of the map on the right ascension (RA) and declination (Dec) direction, it can be fitted by one dimensional Gaussian function to determine the location of the shadow center. Its shift with respect to the normal Moon position is $0.02^\circ \pm 0.03^\circ$ in the Dec direction , while is quite small in the RA direction, i.e, -0.01 ± 0.03. These results of 6 groups is summarized in Table 1, and the statistical uncertainty is the dominant contribution given the limited statistics.

4. Calculation of Moon shadow shifts by raytracing in GMF

In energy scale analysis, it need to know the relationship between energy and deflection angle, it can be obtained by Moon shadow simulation. First of all, this work is simulate the deflection motion of cosmic rays in the magnetic field of Earth and Moon. In this paper, it is assumed that cosmic rays

PoS(ICRC2021)356

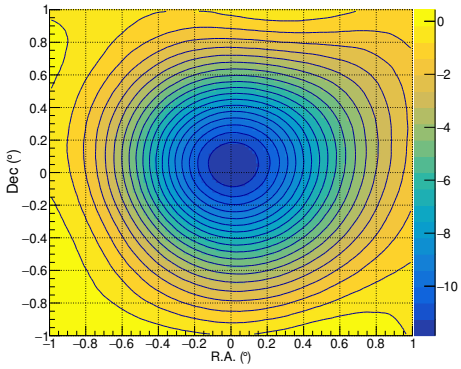

Figure 3: The significance map of Moon shadow for shower events detected by WCDA-1 with $N_{\rm pe} > 60,000$. The deflection of the cosmic rays by the GMF, at such high energies, is seen to be quite small. The coordinates are centered on Moon position. The color scale represents the statistical significance of the deficit in terms of standard deviations.

have hit the detector and traced back to Moon, which greatly improves the simulation efficiency. If the event hits Moon, it can be used as a Moon shadow event. When tracking in the opposite direction, the charge of the cosmic ray particles is opposite to the original charge. In the simulation process, the propagation of primary particles from Moon to Earth is affected by the geomagnetic field and the IGRF model [7] has been used in this work. The Geopack package is called when calculating the magnetic field strength of the geomagnetic field. When the distance from the center of Earth are 1 and 6 radius of Earth, the total intensity distribution of the geomagnetic field given by the IGRF model is shown in Fig. 4. The expected Moon shadow shift westward has been

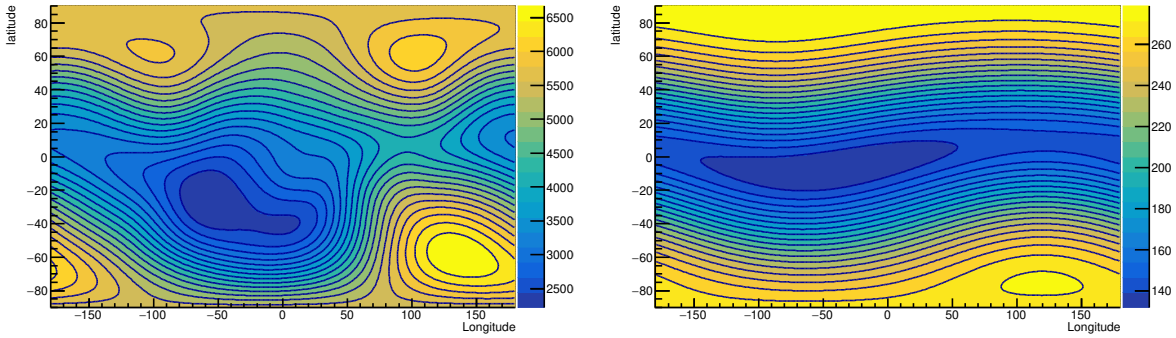

Figure 4: Left:The strength from International Geomagnetic Reference Field model at one Earth radius.Right:The strength from International Geomagnetic Reference Field model at six Earth radius.

calculated by using a ray-tracing simulation which propagates protons and helium nuclei coming from Moon direction through GMF. We find that the displacement obtained applying this model to the propagation of protons and helium nuclei can be represented approximately:

$$\Delta = 1.59^{\circ}/R(TV), \tag{1}$$

PoS(ICRC2021)356

Table 1: Moon shadow shifts in RA, the significance of Moon shadow.

Range of N_{pe}	Shift of the Moon shadow (°)	Significance (σ)
6,000-10,000	-0.32±0.04	18.2
10,000-15,000	-0.25±0.04	14.0
15,000-20,000	-0.15±0.04	11.6
20,000-30,000	-0.11 ±0.03	11.9
30,000-60,000	-0.06 ±0.03	10.8
>60,000	-0.01±0.03	10.9

where R(TV) is the particle rigidity E(TeV)/Z. Thus the expected shift for helium nuclei is a factor of 2 greater than the shift of protons of the same energy. However, for a given energy, the shower size N_e of Helium nuclei is less than the size of proton-induced shower. The median energies and trigger efficiencies of protons and Helium nuclei in a given $N_{\rm pe}$ interval, have been obtained by detailed simulations by CORSIKA v75000 and detector responses. In CORSIKA v75000, the hadronic models EPOS-LHC and FLUKA are selected above and below 100 GeV, respectively [2].

We should also consider the composition and primary protons and helium nuclei and LHAASO-WCDA trigger efficiency in this simulation. The flux of primary protons and helium nuclei is measured already by direct detection experiments, such as CREAM [8] and DAMPE [9] [10] at energies above 1TeV. According to their results, the mixture of protons and helium nuclei is nearly 1:1 from 1.5TeV and 60 TeV. In order to estimate the ratio of protons and helium nuclei after array detection, the simulation of air showers and the WCDA-1 response to the showers is done. It is found the ratio becomes 2:1 with the $N_{\rm hit}$>200 and $N_{\rm pe}$ in the range from 6,000 to 60,000 and the median energy of helium nuclei is 1.9 times that of protons, i.e. $E_{\rm He} \approx 1.9E_{\rm P}$. The change of the ratio is due to two reasons:1) The trigger efficiency of WCDA-1 is slightly different for two types of showers induced by protons and helium nuclei; 2) For showers having a given $N_{\rm pe}$ the energy of He are slightly higher than protons, thus the He flux is lower than that of P in a given $N_{\rm pe}$ range even if full trigger efficiency is achieved. So the amount of the shift is $\Delta = 2.1/E[\rm TeV]$ where E is the median energy of the fixed $N_{\rm pe}$ range.

5. Energy Scale results and summary

As a good approximation, the energy scale is established over the energy range from 6.6 TeV to 35 TeV by using the energy estimator, $N_{\rm pe}$. Results of Moon shadow shifts for each $N_{\rm pe}$ group are shown in Table 1. The median energy and corresponding uncertainty for each point is estimated according to the reversed linear relationship $\Delta = 2.1/E[\rm TeV]$. The best fit with $E[\rm GeV] = \rm bN_{pe}^{\beta}$ are $\beta = 0.95 \pm 0.17$ and $b = 1.33^{+5.26}_{-1.06}$ and the energy scale result in the $N_{\rm pe}$ range 6,000-60,000 is as shown in Fig. 5. The uncertainty of Moon shadow shift can be transferred to the energy scale by using the fact that $d\Delta/\Delta = dE/E$. Therefore, we can obtain the uncertainty in the energy scale from12% at 6.6 TeV to 50% at 35 TeV. There are also some systematic uncertainties should be not neglect. According to simulations, an uncertainty is 3% obtained if the ratio of protons to helium nuclei 10% changing and the uncertainties due to different hadronic models cause less than 2%. In addition, an uncertainty of 4% is caused by energy and angular resolution of the detector.

PoS(ICRC2021)356

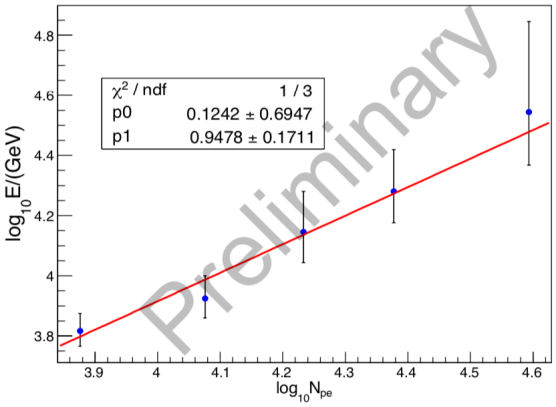

Figure 5: The average shower energy measured using Moon shadow shift versus $N_{\rm pe}$, the total number of photo-electrons detected by WCDA-1 detector.

6. Acknowledgments

The authors would like to thank all staff members who work at the LHAASO site all year around to keep the system running efficiently and smoothly, even in the demanding conditions at a mean altitude of 4400 meters above sea level. We are grateful to the Chengdu Management Committee of Tianfu New Area for the constant financial support to the research with LHAASO data. This research work is also supported by the National Key R&D program of China, with the grant 2018YFA0404201, 2018YFA0404202 and 2018YFA0404203, the National Natural Science Foundation of China, with NSFC grants 11635011, 11761141001, 11905240, 11503021, 11205126, 11947404, 11675187, U1831208, Schools of Science and Technology Plan from SiChuan Province grant No.20SYSX0294, and Thailand Science Research and Innovation grant RTA6280002.

References

[1] B. Bartoli *et al.* (ARGO-YBJ Collaboration), Phys. Rev. **D 84** 022003 (2011)

[2] F. Aharonian*et al.* arXiv:2101.03508v1 [astro-ph.IM]

[3] Z. Cao (for LHAASO Coll.), Chin.Phys. **C34** 249-252 (2010)

[4] H. He (for LHAASO Coll.), Radiation Detection Technology and Methods 2-7, (2018)

[5] M. Amenomori *et al.*, Astrophys. J, **633**, 1005-1012 (2005)

[6] T. P. Li, Y. Q. Ma, 1983, ApJ, 272, 317

[7] N.A. Tsyganenko,J. Geophys. Res.,100, 5599 (1995).

PoS(ICRC2021)356

[8] Y.S.Yoon, et al., Astrophysical J., 839:5 (2017)

[9] Q.An,et al.,Science Advances 5 (9) (2019) eaax3793

[10] F. Alemanno, et al., Phys.Rev.Lett., 126 201102 (2021)

PoS(ICRC2021)356

Full Authors List: LHAASO Collaboration

F. Aharonian[27,28], Q. An[4,5], Axikegu[20], L.X. Bai[21], Y.X. Bai[1,3], Y.W. Bao[15], D. Bastieri[10], X.J. Bi[1,2,3], Y.J. Bi[1,3], H. Cai[23], J.T. Cai[10], Zhen Cao[1,2,3,⋆] Zhe Cao[4,5], J. Chang[16], J.F. Chang[1,3,4], B.M. Chen[13], E.S. Chen[1,2,3], J. Chen[21], Liang Chen[1,2,3], Liang Chen[18], Long Chen[20], M.J. Chen[1,3], M.L. Chen[1,3,4], Q.H. Chen[20], S.H. Chen[1,2,3], S.Z. Chen[1,3], T.L. Chen[22], X.L. Chen[1,2,3], Y. Chen[15], N. Cheng[1,3], Y.D. Cheng[1,3], S.W. Cui[13], X.H. Cui[7], Y.D. Cui[11], B.Z. Dai[24], H.L. Dai[1,3,4], Z.G. Dai[15], Danzengluobu[22], D. della Volpe[32], B. D'Ettorre Piazzoli[29], X.J. Dong[1,3], K.K. Duan[16] J.H. Fan[10], Y.Z. Fan[16], Z.X. Fan[1,3], J. Fang[24], K. Fang[1,3], C.F. Feng[17], L. Feng[16], S.H. Feng[1,3], Y.L. Feng[16], B. Gao[1,3], C.D. Gao[17], L.Q Gao[1,2,3], Q. Gao[22], W. Gao[17], M.M. Ge[24], L.S. Geng[1,3], G.H. Gong[6], Q.B. Gou[1,3], M.H. Gu[1,3,4], F.L. Guo[18], J.G. Guo[1,2,3], X.L. Guo[20], Y.Q. Guo[1,3], Y.Y. Guo[1,2,3,16], Y.A. Han[14], H.H. He[1,2,3], H.N. He[16], J.C. He[1,2,3], S.L. He[10], X.B. He[11], Y. He[20], M. Heller[32], Y.K. Hor[11], C. Hou[1,3], H.B. Hu[1,2,3], S. Hu[21], S.C. Hu[1,2,3], X.J. Hu[6], D.H. Huang[20], Q.L. Huang[1,3], W.H. Huang[17], X.T. Huang[17], X.Y.Huang[16], Z.C. Huang[20], F. Ji[1,3], X.L. Ji[1,3,4], H.Y. Jia[20], K. Jiang[4,5], Z.J. Jiang[24], C. Jin[1,2,3], T. Ke[1,3], D. Kuleshov[30], K. Levochkin[30], B.B. Li[13], Cong Li[1,3], Cheng Li[4,5], F. Li[1,3,4], H.B. Li[1,3], H.C. Li[1,3], H.Y. Li[5,16], J. Li[1,3,4], K. Li[1,3], W.L. Li[17], Xin Li[4,5], Xin Li[20], X.R. Li[1,3], Y. Li[21], Y.Z. Li[1,2,3], Zhe Li[1,3], Zhuo Li[9], E.W. Liang[12], Y.F. Liang[12], S.J. Lin[11], B. Liu[5], C. Liu[1,3], D. Liu[17], H. Liu[20], H.D. Liu[14], J. Liu[1,3], J.L. Liu[19], J.S. Liu[11], J.Y. Liu[1,3], M.Y. Liu[22], R.Y. Liu[15], S.M. Liu[20], W. Liu[1,3], Y. Liu[10], Y.N. Liu[6], Z.X. Liu[21], W.J. Long[20], R. Lu[24], H.K. Lv[1,3], B.Q. Ma[9], L.L. Ma[1,3⋆], X.H. Ma[1,3], J.R. Mao[25], A. Masood[20], Z. Min[1,3] W. Mitthumsiri[33], T. Montaruli[32], Y.C. Nan[17⋆], B.Y. Pang[20], P. Pattarakijwanich[33], Z.Y. Pei[10], M.Y. Qi[1,3], Y.Q. Qi[13], B.Q. Qiao[1,3], J.J. Qin[5] D. Ruffolo[33], V. Rulev[30], A. Sáiz[33], L. Shao[13], O. Shchegolev[30,31], X.D. Sheng[1,3], J.Y. Shi[1,3], H.C. Song[9], Yu.V. Stenkin[30,31], V. Stepanov[30], Y. Su[16] Q.N. Sun[20], X.N. Sun[12], Z.B. Sun[8], P.H.T. Tam[11], Z.B. Tang[4,5], W.W. Tian[2,7], B.D. Wang[1,3], C. Wang[8], H. Wang[20], H.G. Wang[10], J.C. Wang[25], J.S. Wang[19], L.P. Wang[17], L.Y. Wang[1,3], R.N. Wang[20], W. Wang[11], W. Wang[23], X.G. Wang[12], X.J. Wang[1,3], X.Y. Wang[15], Y. Wang[20] Y.D. Wang[1,3], Y.J. Wang[26⋆], Y.P. Wang[1,2,3], Z.H. Wang[21], Z.X. Wang[24], Zhen Wang[19], Zheng Wang[1,3,4], D.M. Wei[16], J.J. Wei[16], Y.J. Wei[1,2,3], T. Wen[24], C.Y. Wu[1,3], H.R. Wu[1,3], S. Wu[1,3], W.X. Wu[20], X.F. Wu[16], S.Q. Xi[1,3], J. Xia[5,16], J.J. Xia[20], G.M. Xiang[2,18], D.X. Xiao[22] G. Xiao[1,3], H.B. Xiao[10], G.G. Xin[23], Y.L. Xin[20], Y. Xing[18], D.L. Xu[19], R.X. Xu[9], L. Xue[17], D.H. Yan[25], J.Z. Yan[16] C.W. Yang[21], F.F. Yang[1,3,4], J.Y. Yang[11], L.L. Yang[11], M.J. Yang[1,3], R.Z. Yang[5], S.B. Yang[24], Y.H. Yao[21], Z.G. Yao[1,3], Y.M. Ye[6], L.Q. Yin[1,3], N. Yin[17], X.H. You[1,3], Z.Y. You[1,2,3], Y.H. Yu[17], Q. Yuan[16], H.D. Zeng[16], T.X. Zeng[1,3,4], W. Zeng[24], Z.K. Zeng[1,2,3⋆], M. Zha[1,3], X.X. Zhai[1,3], B.B. Zhang[15], H.M. Zhang[15], H.Y. Zhang[17], J.L. Zhang[7], J.W. Zhang[21], Lu Zhang[13], Li Zhang[24], L.X. Zhang[10], P.F. Zhang[24], P.P. Zhang[13], R. Zhang[5,16], S.R. Zhang[13], S.S. Zhang[1,3], X. Zhang[15], X.P. Zhang[1,3], Y.F. Zhang[20], Y.L. Zhang[1,3], Yong Zhang[1,3], Yi Zhang[1,16], B. Zhao[20], J. Zhao[1,3], L. Zhao[4,5], L.Z. Zhao[13], S.P. Zhao[16,17], F. Zheng[8], Y. Zheng[20], B. Zhou[1,3], H. Zhou[19], J.N. Zhou[18], P. Zhou[15], R. Zhou[21], X.X. Zhou[20], C.G. Zhu[17], F.R. Zhu[20], H. Zhu[7], K.J. Zhu[1,2,3,4], X. Zuo[1,3]

[1] Key Laboratory of Particle Astrophyics & Experimental Physics Division & Computing Center, Institute of High Energy Physics, Chinese Academy of Sciences, 100049 Beijing, China

[2]University of Chinese Academy of Sciences, 100049 Beijing, China

[3]TIANFU Cosmic Ray Research Center, Chengdu, Sichuan, China

[4]State Key Laboratory of Particle Detection and Electronics, China

[5]University of Science and Technology of China, 230026 Hefei, Anhui, China

[6]Department of Engineering Physics, Tsinghua University, 100084 Beijing, China

[7]National Astronomical Observatories, Chinese Academy of Sciences, 100101 Beijing, China

[8]National Space Science Center, Chinese Academy of Sciences, 100190 Beijing, China

[9]School of Physics, Peking University, 100871 Beijing, China

[10]Center for Astrophysics, Guangzhou University, 510006 Guangzhou, Guangdong, China

[11]School of Physics and Astronomy & School of Physics (Guangzhou), Sun Yat-sen University, 519082 Zhuhai, Guangdong, China

[12]School of Physical Science and Technology, Guangxi University, 530004 Nanning, Guangxi, China

[13]Hebei Normal University, 050024 Shijiazhuang, Hebei, China

[14]School of Physics and Microelectronics, Zhengzhou University, 450001 Zhengzhou, Henan, China

[15]School of Astronomy and Space Science, Nanjing University, 210023 Nanjing, Jiangsu, China

[16]Key Laboratory of Dark Matter and Space Astronomy, Purple Mountain Observatory, Chinese Academy of Sciences, 210023 Nanjing, Jiangsu, China

[17]Institute of Frontier and Interdisciplinary Science, Shandong University, 266237 Qingdao, Shandong, China

[18]Key Laboratory for Research in Galaxies and Cosmology, Shanghai Astronomical Observatory, Chinese Academy of Sciences, 200030 Shanghai, China

[19]Tsung-Dao Lee Institute & School of Physics and Astronomy, Shanghai Jiao Tong University, 200240 Shanghai, China

[20]School of Physical Science and Technology & School of Information Science and Technology, Southwest Jiaotong University, 610031 Chengdu, Sichuan, China

[21]College of Physics, Sichuan University, 610065 Chengdu, Sichuan, China

[22]Key Laboratory of Cosmic Rays (Tibet University), Ministry of Education, 850000 Lhasa, Tibet, China

[23]School of Physics and Technology, Wuhan University, 430072 Wuhan, Hubei, China

[24]School of Physics and Astronomy, Yunnan University, 650091 Kunming, Yunnan, China

[25]Yunnan Observatories, Chinese Academy of Sciences, 650216 Kunming, Yunnan, China

[26]College of Sciences, Northeastern University, 110819 Shenyang, Liaoning, China

[27]Dublin Institute for Advanced Studies, 31 Fitzwilliam Place, 2 Dublin, Ireland

[28]Max-Planck-Institut for Nuclear Physics, P.O. Box 103980, 69029 Heidelberg, Germany

PoS(ICRC2021)356

[29] Dipartimento di Fisica dell'Università di Napoli "Federico II", Complesso Universitario di Monte Sant'Angelo, via Cinthia, 80126 Napoli, Italy.
[30]Institute for Nuclear Research of Russian Academy of Sciences, 117312 Moscow, Russia
[31]Moscow Institute of Physics and Technology, 141700 Moscow, Russia
[32]Département de Physique Nucléaire et Corpusculaire, Faculté de Sciences, Université de Genève, 24 Quai Ernest Ansermet, 1211 Geneva, Switzerland
[33]Department of Physics, Faculty of Science, Mahidol University, 10400 Bangkok, Thailand

PoS(ICRC2021)356